energy&fuels

pubs.acs.org/EF

Article

Toward a More Comprehensive Understanding of the Kinetics of a Common Biomass-Derived Impurity: NH_3 Oxidation by N_2O in a Jet-Stirred Reactor

Rodger E. Cornell, Mark C. Barbet, and Michael P. Burke*

Cite This: *Energy Fuels* 2021, 35, 13338−13348

Read Online

ACCESS | Metrics & More | Article Recommendations | Supporting Information

ABSTRACT: Ammonia (NH_3) has garnered substantial attention in recent years due to its importance across many scientific and engineering domains—including its potential use as a carbon-free fuel and long-term energy storage option, its use in reducing combustion-generated nitrogen oxide emissions, its role as a decomposition fragment of many energetic materials, and its presence as an important impurity during biofuel and biomass combustion that can affect overall system kinetics, among others. Yet, it is generally recognized that there are still significant gaps in the present understanding of ammonia kinetics—in both experimental data sets and submodels within the overall ammonia kinetic mechanism. For example, most experimental studies of ammonia oxidation have used molecular oxygen as the primary or sole oxidizer. While large mole fractions of molecular oxygen are encountered in many combustion scenarios, there are select systems where ammonia is more likely to be oxidized via nitrogen-containing species (e.g., N_2O), and, more generally, there are relatively untested reaction sets that would be accentuated in such conditions. To address one such gap in experimental data sets for the validation of ammonia kinetics submodels, we present results from jet-stirred reactor experiments of an $NH_3/N_2O/N_2$ mixture over an intermediate temperature range (850−1180 K). In these experiments, the mole fractions of NH_3, N_2O, and NO are measured through a combination of gas chromatography, chemiluminescence, electrochemical detection, and infrared absorption—where agreement among the different diagnostics (within 3% for N_2O and 7% for NO) ensures high confidence in the experimental measurements. Comparison of the experimental results and model predictions suggests deficiencies in commonly used models for nitrogen kinetics. Various modeling analyses point to the central role of the $N_2O + NH_2 = N_2H_2 + NO$ reaction, on which recent kinetic models all rely on the same rate constant estimate that appears to have not been tested in previous validation data sets for NH_3 kinetics.

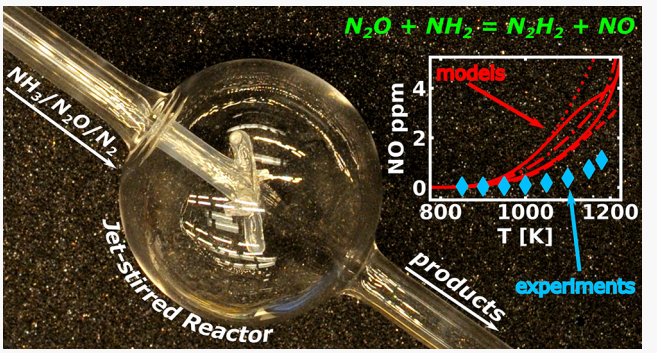

INTRODUCTION

Ammonia (NH_3) kinetics has received significant attention due to its broad relevance across many scientific and engineering domains.[1−8] Important applications include, for example, its proposed use as a carbon-free energy carrier,[1,2,7] its continued use as a nitrogen oxide reduction agent in the thermal DeNO$_x$ process[9−12] and similar processes using urea,[13] its role as a decomposition fragment of many energetic materials,[14−18] and its presence in trace quantities as an impurity during biofuel and biomass combustion that influences overall system kinetics.[4,19−21] As the breadth of its applications continues to grow, there is an increasing need for comprehensive ammonia kinetic models that can accurately predict its kinetics across such highly varied domains with confidence. Even with the substantial previous attention devoted to ammonia kinetics, many researchers still believe that our understanding of ammonia chemistry is incomplete.[11,22−24] For example, Stagni et al.[23] note that "a comprehensive understanding of its kinetic behavior is still an open challenge, especially at low temperature (T < 1200 K) and under diluted conditions." Indeed, many submodels within NH_3 kinetic mechanisms rely on rate constant estimates that likely have not been tested/validated in previous theoretical and experimental studies.

For example, most prior experimental studies of ammonia oxidation involve large mole fractions of molecular oxygen as it is readily available during many combustion processes.[11,25−35] Among those experimental studies, trace amounts of nitrogen oxides (NO, NO_2, N_2O) are often included as reactants (in addition to O_2) given their presence in many ammonia

Received: May 18, 2021
Revised: July 14, 2021
Published: July 30, 2021

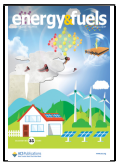

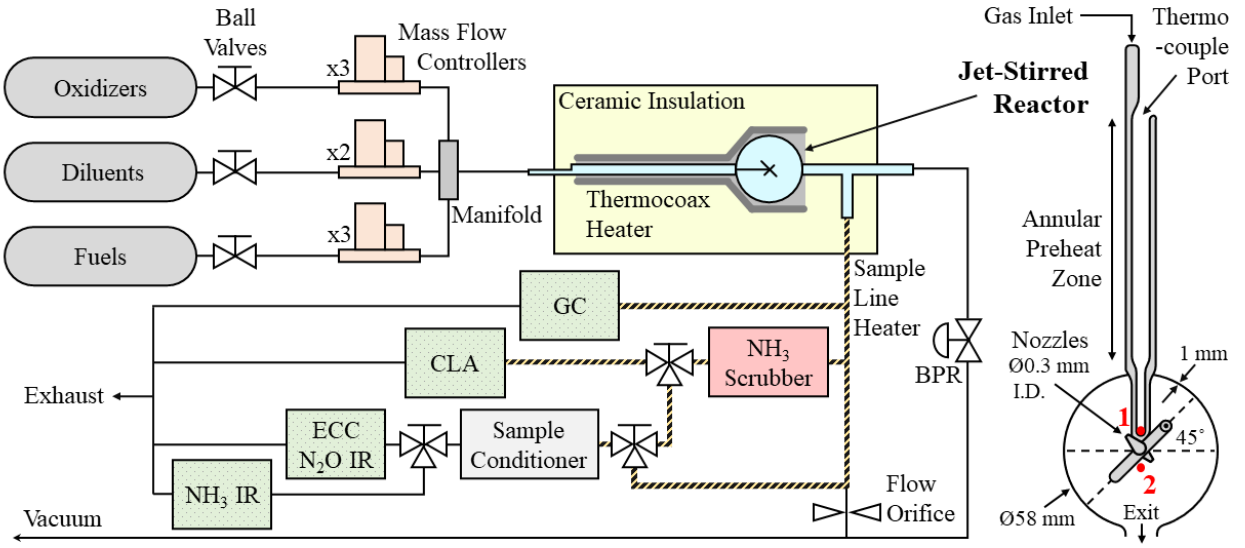

Figure 1. Simplified schematic of the 1 atm jet-stirred reactor system used for this study (located at Columbia University). Thermocouple locations (1, 2) are shown in the magnified JSR image on the right side of the figure. Note that only one MFC was utilized for this study given that a single certified standard gas tank contained the reactant mixture.

applications, notably the thermal DeNO$_x$ process and biomass combustion.[12,36−38] However, experimental studies of ammonia oxidation by nitrogen-containing species (e.g., NO, NO$_2$, N$_2$O) in the absence of O$_2$ are much more limited[39,40] — particularly for N$_2$O, which has generally been studied only at higher temperatures (above 1500 K).[41−43] Consequently, new experimental data for such reactant mixtures would be valuable for establishing ammonia kinetic models that can be broadly used across varied application domains by both evaluating untested reaction sets and accentuating different combinations of rate constants than previous data sets.

Additionally, in some applications (e.g., during the combustion of nitrogen-rich energetic materials[14,15]), ammonia is exclusively oxidized in an environment where nitrogen-containing oxidizers are present in much higher mole fractions than O$_2$. Furthermore, NH$_3$/N$_2$O kinetics is also expected to be relevant to biomass combustion, where NH$_3$ and N$_2$O are often present in sizable fractions,[21] and to nitrogen oxide reduction strategies using ammonia, where N$_2$O is both an undesirable byproduct in NO$_x$ reduction applications[10] and itself among the major nitrogen oxide emissions in fluidized bed combustion.[44] In fact, deficiencies in model predictions of N$_2$O during thermal deNO$_x$ under low O$_2$ mole fractions in particular have been highlighted in recent studies.[11,12,27] Therefore, experimental data for NH$_3$/N$_2$O kinetics are important for the validation of broadly applicable nitrogen kinetics models for these and other applications. To address this gap in the available experimental data sets for ammonia oxidation kinetics, we perform jet-stirred reactor (JSR) experiments for a NH$_3$/N$_2$O/N$_2$ mixture at intermediate temperatures (850−1180 K). Gas chromatography, chemiluminescence, electrochemical detection, and infrared absorption are used to gather species mole fraction data for NH$_3$, NO, and N$_2$O. All results are compared against simulation predictions using five recent kinetic models.[11,23,24,45,46] These comparisons reveal significant differences between experimental measurements and predictions using recent kinetic models, suggesting deficiencies in submodels for NH$_3$/N$_2$O kinetics. These discrepancies are investigated through a combination of flux analysis, uncertainty-weighted kinetic sensitivity analysis, and other analyses to identify the influential reactions in this experimental system. These analyses point to the central role of the NH$_2$ + N$_2$O = N$_2$H$_2$ + NO reaction, on which recent kinetic models all rely on the same estimate. We then present modeling results that suggest that this reaction has remained untested in previous validation data sets for NH$_3$ kinetics along with a discussion of the conditions under which it may play a role.

EXPERIMENTAL METHODS

To quantitatively assess NH$_3$/N$_2$O kinetics over an intermediate temperature range, experiments are performed using the jet-stirred reactor (JSR) facility at Columbia University (Figure 1) at the conditions specified in Table 1. The JSR facility consists of a flow delivery system that can prepare mixtures of several gases, a temperature-controlled JSR, and several online fast-response diagnostics that enable simultaneous measurements of multiple species. Of note, all components are controllable by computer to enable later planned high-throughput and/or automated operation at experimental conditions selected by Bayesian Design of Experiments.[47]

Table 1. Experimental Conditions with Estimated Uncertainties

mixture composition	444.4 ppm of NH$_3$ (±2%) 951.1 ppm of N$_2$O (±2%) balance N$_2$
residence time	1.2 s (±5%)
pressure	1.02 atm (±1%)
temperature	850−1180 K (±1%)

The flow delivery system consists of Bronkhorst EL-FLOW Prestige mass flow controllers (MFCs) followed by a mixing manifold upstream of the reactor. In this study, in order to reduce reactant mixture composition uncertainties, a certified standard gas mixture of NH$_3$/N$_2$O/N$_2$, whose composition and specified uncertainties are provided in Table 1, was directly flowed from a single MFC. Volumetric flow rates were in the range of 0.9882−1.3718 ± 0.0095 L/min to yield a constant nominal residence time inside the JSR of 1.2 s across all temperatures.

The quartz JSR used for this study is based on the design of Herbinet et al.,[48,49] which is in turn based on the design principles of

https://doi.org/10.1021/acs.energyfuels.1c01544
Energy Fuels 2021, 35, 13338−13348

Matras and Villermaux,[50] has been found to closely mimic key behavior of a perfectly stirred reactor,[51,52] and has been used for many kinetic studies.[48,49,53−56] Before entering the spherical reactor, the reactant mixture is rapidly preheated in a thin annular preheating zone with large surface area to maintain thermal homogeneity inside the reactor[57] and with small volume to limit the extent of reaction prior to the entrance into the reactor.[48,58] The preheated mixture is then ejected into the spherical reactor (nominally 56 mm diameter) via four quartz nozzles (0.25−0.30 mm inner diameter) in a crossed configuration angled 45° from the equatorial plane to promote rapid, turbulent mixing and high recirculation ratios to yield high spatial homogeneity throughout the reactor volume. Previous experimental and computational studies[51,52] have found that this particular reactor configuration[48,49] produces nearly ideal residence time distributions and spatial homogeneity within its designed range of residence times. The nominal residence time inside the reactor is specified by the reactor volume divided by the volumetric flow rate of the reactant mixture. Water displacement measurements of our reactor indicate an internal reactor volume of 82 ± 2 cm^3. On the basis of the uncertainties in the reactor volume and the flow rate (discussed above), the estimated uncertainty in the nominal residence time is approximately ±5%.

System temperature is maintained using a Thermocoax resistive heating element coiled around the reactor and preheating zone. Surrounding the heating element is 75−100 mm thick ceramic insulation that allows for a peak reactor temperature slightly above 1200 K. Temperature is measured simultaneously at two reactor locations (Figure 1) using independent Omega high-temperature, low-drift K-type thermocouple probes (SCAXL-062), which are rated to have ≤±1.5 K noise, ≤±1.5 K deviations from linearity, and ≤±2.8 K calibration drift. The first probe (labeled "1" in Figure 1) monitors the temperature near the nozzle inlets via an inner concentric access port positioned inside the annular preheating zone. The second probe (labeled "2" in Figure 1), which is encased within a 2 mm quartz capillary tube, monitors temperature within the spherical reactor via the reactor outlet tube and can translate along its center line to observe spatial gradients in the temperature profile. Preliminary testing with pure Ar has shown that spatial temperature deviations within the reactor are typically limited to ≤±5 K when testing in the range of 850−1180 K. The low reactant mole fractions and low extent of reaction explored in this study also limit reaction exothermicity, thereby introducing minimal additional spatial temperature deviations due to reaction. (Indeed, even adiabatic simulations at the present conditions suggest a maximum temperature rise of 3 K.) Similarly, temporal profiles of recorded temperatures shown in Figure 2 for a fixed thermocouple position near the center of the spherical reactor (thermocouple location 2 of Figure 1) for each temperature set point indicate temporal variations of ≤±2 K. Altogether, the estimated uncertainty in the reactor temperature is approximately ±1% of each temperature set point.

The gas mixture exiting the reactor is split between an exhaust line, which is used to control the pressure, and a sampling line, which carries a portion of the flow to the online species diagnostics. Reactor pressure is controlled using an Equilibar dome-loaded back pressure regulator (BPR) located in the exhaust line. Reactor pressure is maintained slightly above atmospheric at 1.02 atm to suppress N_2 and O_2 sample contamination from the surrounding air. The exhaust line downstream of the BPR is held at a slight vacuum near 0.27 atm to provide a sufficient pressure gradient across the BPR needed for responsive pressure control. An Omega high-accuracy, digital pressure gauge (DPG409-030A) is positioned at the beginning of the exhaust line to monitor reactor pressure and provide a voltage output signal to the BPR's PID controller to maintain 1.02 atm as flow conditions vary. Pressure measurements indicate variations of less than 0.0007 atm from the set point. Based on the specified uncertainties for the pressure gauge of ±0.0007 atm noise, ±0.0014 atm accuracy, and ±0.0021 atm stability, the estimated uncertainty in the pressure is less than ±1%.

The gas mixture exiting the reactor is sampled through silica-coated stainless-steel tubes maintained near 385 K using a secondary resistive

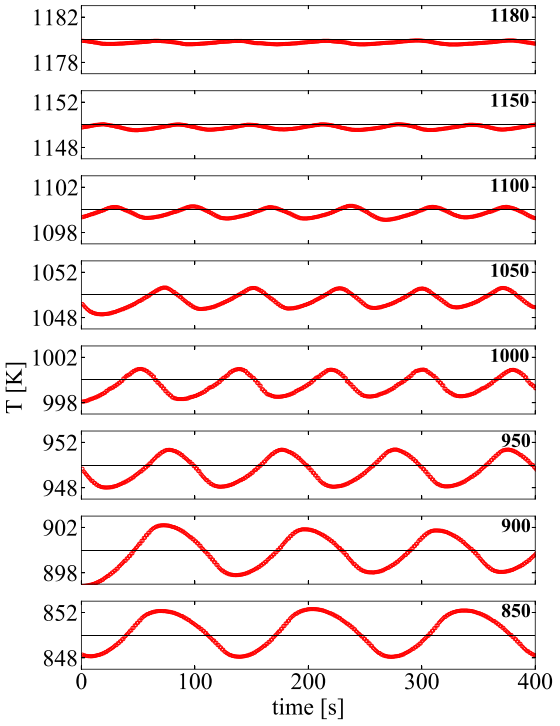

Figure 2. Measured temperature profiles at a fixed thermocouple location near the center of the spherical reactor. Temperature set points are listed in bold font in the upper right corner of each subplot. All subplot temperature scales are set to ±3 K of the set point.

"sample line heater" to prevent water and any other low-volatility products from condensing out of the gas-phase mixture. Four independent diagnostics sample from this gaseous mixture to measure species mole fractions at each experimental condition. An Eco Physics AG NO_x chemiluminescence analyzer (CLA) and an Infrared Industries NO electrochemical cell (ECC) measure NO, an Infrared Industries IR-208 gas analyzer (IR) and an Inficon Micro GC Fusion gas analyzer (GC) measure N_2O, and a secondary Infrared Industries IR-208 gas analyzer measures NH_3. While the GC is capable of measuring many other species, notably H_2 and O_2, these molecules remain below detectable mole fraction limits during all conducted experiments. The CLA and GC analyzers draw adequate sample flow via their respective internal pumps while the IR and ECC detectors rely upon an external sample conditioner that generates stable flow and simultaneously removes any particulates and water from the sample stream.

Prior to its entry to the CLA, ECC, and N_2O IR detectors, the sampled flow is first passed through a heated (∼400 K) PermaPure AS series NH_3 scrubber. In the case of the CLA, the removal of NH_3 was found to eliminate large calibration drifts observed in earlier experiments performed without the scrubber. In the case of the ECC and IR detectors, the removal of NH_3 avoids known compatibility issues with components in those devices. This scrubber contains phosphoric acid, which reacts with NH_3 in the sample flow to form ammonium phosphate—a high melting point salt that is deposited in the scrubber. (As a cautionary note, while this reaction is intended to be highly selective and only affect NH_3 mole fractions, the authors have observed the scrubber reduce NO_2 mole fractions in a separate experiment. However, this is of little concern here as NO_2 mole fractions are expected to remain below detectable mole fractions at the present experimental conditions.)

Species measurements in the gases sampled from the reactor were taken for reactor temperatures spanning 850−1180 K in 50 K increments except for the highest temperature. At each temperature set point, measurements were taken for at least 10−15 min to confirm that steady-state conditions had been reached. Each device was

https://doi.org/10.1021/acs.energyfuels.1c01544
Energy Fuels 2021, 35, 13338−13348

Table 2. Measurement Uncertainties Specific to Each Diagnostic

	NO (CLA)	NO (ECC)	N_2O (IR)	N_2O (GC)	NH_3 (IR)
calibration gas	4.77 ppm	49.37 ppm	773.3 ppm	773.3 ppm	444.4 ppm
	±5%	±2%	±2%	±2%	±2%
calibration drift	+4%	+11%	+1%	+1%	+6%
	0%	−11%	−1%	0%	−2%
signal noise (1σ)	±1%	±10%	±1%	±1%	±1%
minimum uncertainty	±0.03 ppm	±0.30 ppm	±3.9 ppm	±8.4 ppm	±2.2 ppm

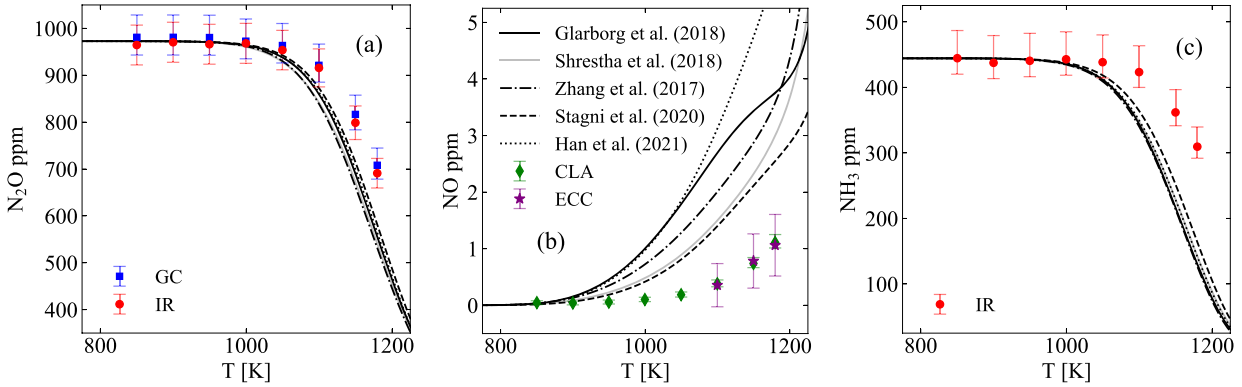

Figure 3. Experimental measurements and model predictions of (a) N_2O, (b) NO, and (c) NH_3 for conditions shown in Table 1.

calibrated using certified standard mixtures acquired from Airgas with specified uncertainties listed in Table 2. A multipoint calibration was performed for the GC measurements of N_2O over a mole fraction range that encompassed the full mole fraction range relevant to this study.

Calibrations were tested after taking measurements to quantify any drift in the calibration. For the GC, CLA, and ECC, calibrations were performed before any measurements were taken and then tested after all measurements were taken. For the IR diagnostics (which experience larger drift), after measurements were taken at each temperature set point, the calibration drift for each was quantified, and then calibrations were repeated by feeding calibration gas directly into each detector. For each diagnostic, the maximum calibration drift observed between calibrations is reported in Table 2 along with the measured noise among multiple measurements at each set point and the minimum uncertainty due to resolution and linearity limitations. The uncertainties for each measured species for each diagnostic from Table 2 are then combined to produce the error bars shown in Figures 3 and 6.

Experiments were performed across the full temperature range twice with ∼72 h between experimental runs to investigate measurement repeatability and satisfy flow requirements for each diagnostic. In the first run, N_2O and NO were measured using the IR and ECC, respectively; in the second run, N_2O, NO, and NH_3 were measured using the GC, CLA, and IR, respectively. Only data above the ECC's minimum resolution (0.3 ppm) are shown in Figures 3 and 6.

SIMULATION METHODS

Simulations in an isothermal, isobaric, perfectly stirred reactor were performed in Cantera 2.4.0[59] using an ideal gas equation of state and five recently developed kinetic models. These include the model of Zhang et al.[45] for NO_x kinetics and the model of Glarborg et al.[11] for nitrogen kinetics, both of which contain submodels for NH_3 oxidation kinetics. Also included are the models of Shrestha et al.,[46] Stagni et al.,[23] and Han et al.[24] for NH_3 oxidation kinetics. To facilitate comparisons between model predictions and experimental measurements for N_2O consumption, in the simulations shown in Figures 3 and 6, the measured N_2O mole fraction at low temperatures (977 ppm) is used as the N_2O mole fraction in the simulated reactant mixture instead of the value specified in the certified standard gas mixture used as the reactant mixture (951 ppm) (though the two agree within the 2% N_2O mole fraction uncertainties in each of the two different certified standard gas mixtures). For the uncertainty-weighted kinetic sensitivity analyses, the most recently recommended uncertainty factor for each reaction among various rate constant evaluations[60−64] is used.

RESULTS AND DISCUSSION

Experimental measurements and model predictions of N_2O, NO, and NH_3 mole fractions are shown in Figure 3. As observed in Figure 3a and b, there is excellent agreement between GC and IR measurements of N_2O (within 3%) and CLA and ECC measurements of NO (within 7%). Not only do these data suggest a high level of consistency of the experimental measurements among diagnostics, but also they suggest that experimental repeatability is very good as the GC and IR measurements of N_2O and the CLA and ECC measurements of NO were taken on different days.

The measurements and predictions of all four models indicate an onset of N_2O and NH_3 consumption near 1000 K, albeit with model predictions for all models showing a faster rate of consumption than observed experimentally, particularly for NH_3. On the contrary, model predictions suggest an onset for NO formation at temperatures as low as ∼900 K with a sharp rise thereafter with increasing temperature, whereas experimental measurements indicate an onset of NO formation at temperatures closer to 1000−1100 K. At temperatures above 900 K, predicted NO mole fractions for all models are higher than experimental measurements by as much as an order of magnitude.

Flux analysis performed using the model of Glarborg et al.[11] at the present conditions (Figure 4) suggests that N_2O (Figure 4a) is primarily consumed by unimolecular decomposition

$$N_2O(+M) \Leftrightarrow N_2 + O(+M) \quad (1)$$

and bimolecular reactions with H and NH_2

https://doi.org/10.1021/acs.energyfuels.1c01544
Energy Fuels 2021, 35, 13338−13348

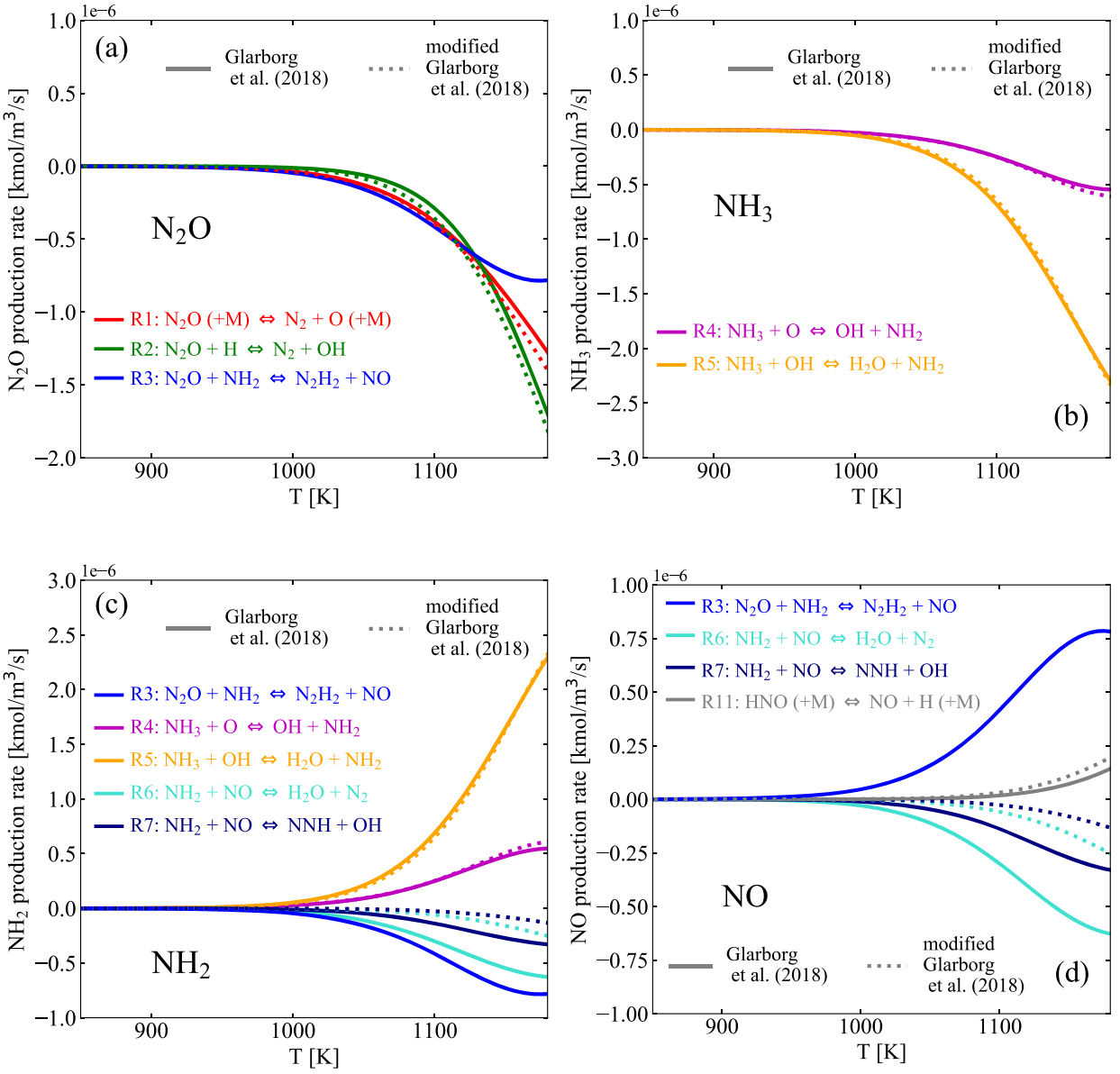

Figure 4. Rate of production for (a) N_2O, (b) NH_3, (c) NH_2, and (d) NO by each reaction calculated using the model of Glarborg et al.[11] (solid lines) and a modified version of the same model without R3 (dotted lines).

$$N_2O + H \Leftrightarrow N_2 + OH \quad (2)$$

$$N_2O + NH_2 \Leftrightarrow N_2H_2 + NO \quad (3)$$

to produce O and OH radicals, which are the coreactants in the two primary NH_3 consumption reactions (Figure 4b)

$$NH_3 + O \Leftrightarrow OH + NH_2 \quad (4)$$

$$NH_3 + OH \Leftrightarrow H_2O + NH_2 \quad (5)$$

that are also the primary production reactions for NH_2 (Figure 4c), which is in turn primarily consumed by reactions with N_2O (R3) and NO

$$NH_2 + NO \Leftrightarrow H_2O + N_2 \quad (6)$$

$$NH_2 + NO \Leftrightarrow NNH + OH \quad (7)$$

where the NNH quickly decomposes to H and N_2, making the latter the key chain-branching reaction at these conditions (similar to other situations involving NH_3[11]). At higher temperatures, the analysis using the model of Glarborg et al.[11] suggests that reactions of NH_2 with other radicals (O, H, and NH) including

$$NH_2 + O \Leftrightarrow H + HNO \quad (8)$$

$$NH_2 + H \Leftrightarrow H_2 + NH \quad (9)$$

$$NH_2 + NH \Leftrightarrow H + N_2H_2 \quad (10)$$

also play a role in NH_2 consumption, though they are still much less prominent than R3, R6, and R7—at least when using rate constant values for R3 contained in present models (as discussed further below).

Figure 4d indicates that both production and consumption of NO predicted using the model of Glarborg et al.[11] are nearly exclusively due to reactions involving NH_2 as a reactant. Namely, reaction of NH_2 with N_2O (R3) is nearly exclusively responsible for NO production, and reactions of NH_2 with NO (R6, R7) are nearly exclusively responsible for NO

https://doi.org/10.1021/acs.energyfuels.1c01544
Energy Fuels 2021, 35, 13338−13348

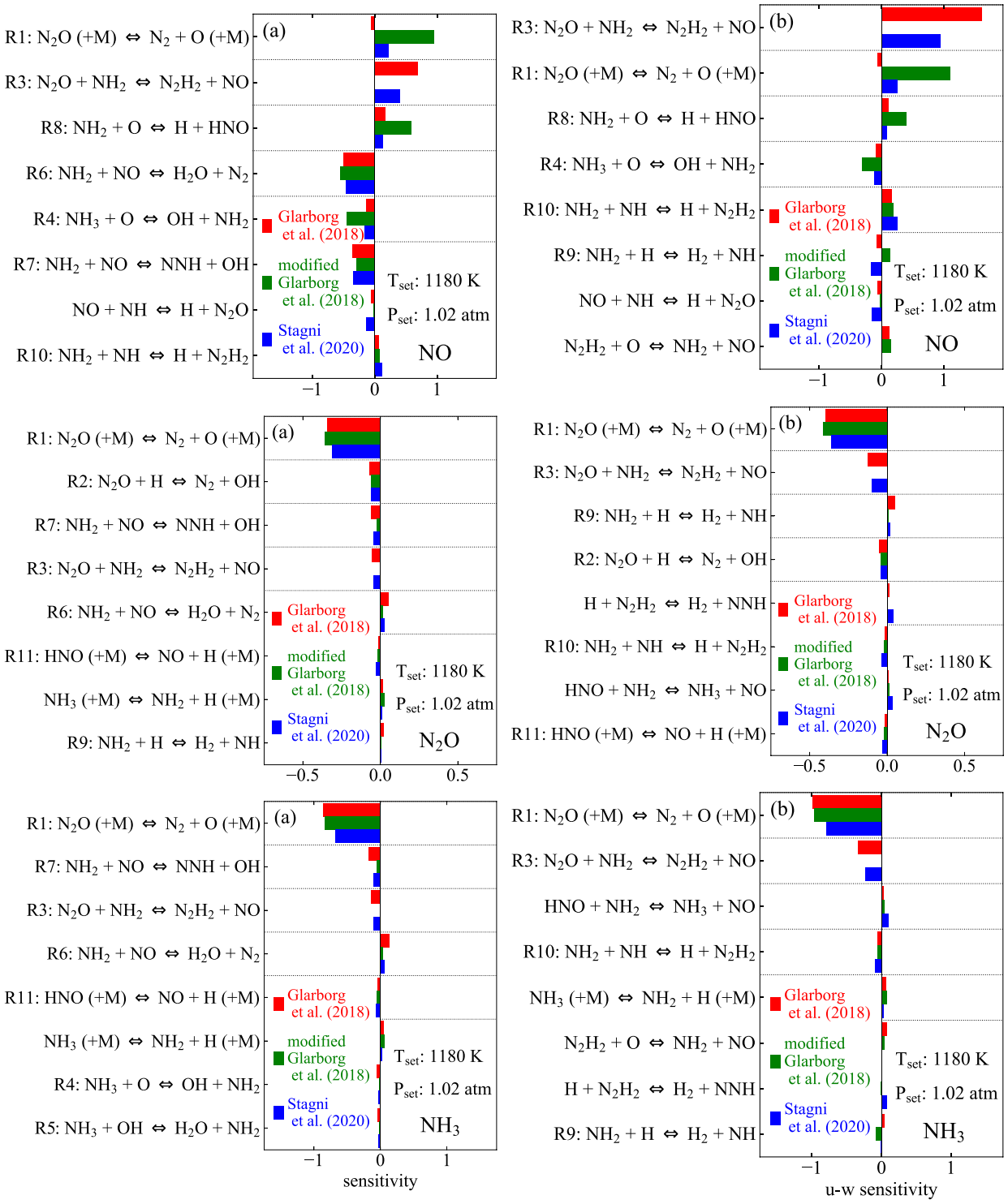

Figure 5. Results from (a) sensitivity and (b) uncertainty-weighted (u-w) sensitivity analysis for NO, N_2O, and NH_3 mole fractions at 1180 K using two recent models[11,23] and a modified version of Glarborg et al.[11] with R3 removed.

consumption. In fact, predictions of the NO/N_2O ratio using the model of Glarborg et al.[11] are nearly identical to the ratio of $k_3/(k_6 + k_7)$ across the full temperature range here, consistent with NO reaching a quasi-steady-state mole fraction based on production by R3 and rapid consumption by R6 and R7.

To explore the possible sources of the discrepancies between model predictions and experimental measurements, the sensitivity of predicted mole fractions of species i to rate constants for each reaction j, $\partial\ln(X_i)/\partial\ln(k_j)$, were calculated. The results of this sensitivity analysis at 1180 K using the models of Glarborg et al.[11] and Stagni et al.[23] are depicted in Figure 5a. The results for the two models both indicate that predictions of all three species are most sensitive to R1, R3, R6, and R7.

https://doi.org/10.1021/acs.energyfuels.1c01544
Energy Fuels 2021, 35, 13338−13348

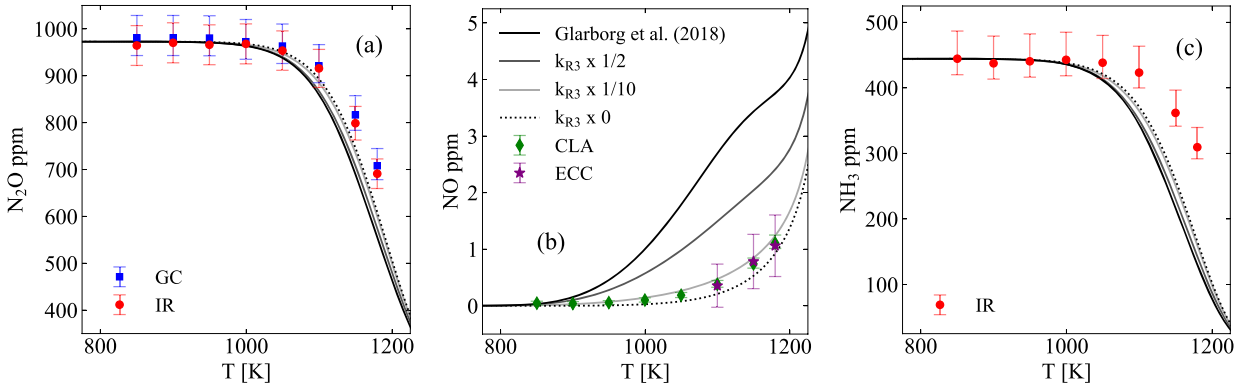

Figure 6. Experimental measurements and model predictions of (a) N_2O, (b) NO, and (c) NH_3 using the model of Glarborg et al.[11] and modified versions of the same model with reduced rate constant values for R3.

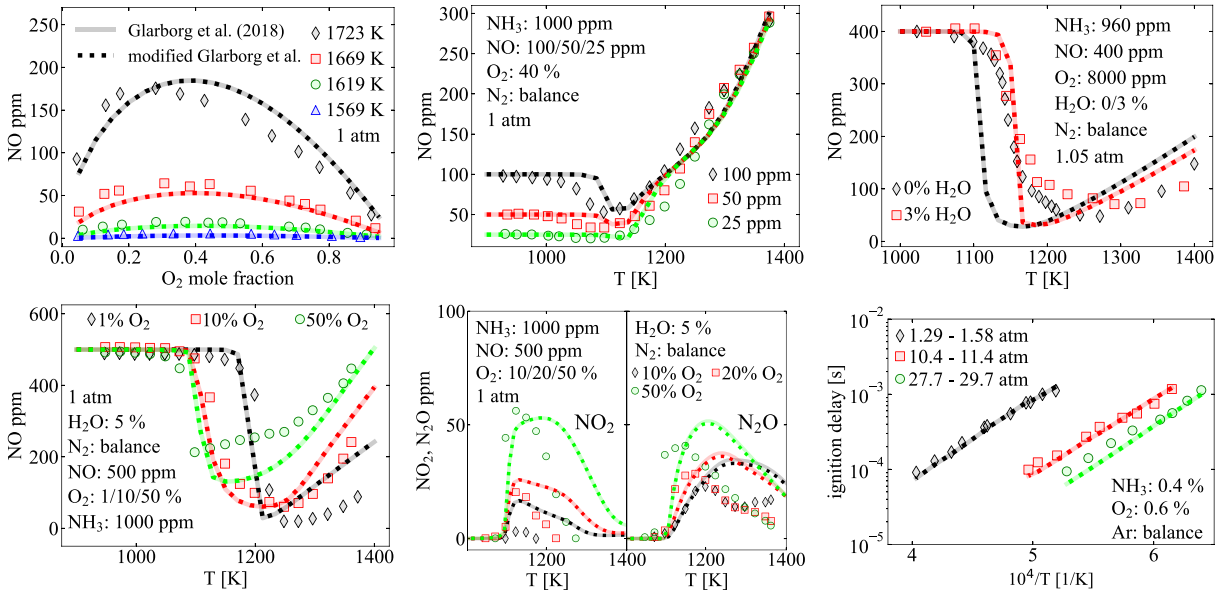

Figure 7. Comprehensive validation data set for NH_3/NO_x kinetics over a wide range of temperature (900−2000 K) and pressure (1−30 atm). Symbols represent experimental measurements.[12,32,37,65] Solid lines represent predictions using the model of Glarborg et al.,[11] while dotted lines represent a modified version of the same model without R3.

While reactions R1, R6, and R7 have been thoroughly investigated in numerous prior studies, R3 has received far less attention. A closer look at the rate parameters in each model show that all five models use the same estimated rate constant for R3—an approximation of Dean and Bozzelli[29] based on NO addition to N_2H_2 being similar to NO addition to HNO. Recognizing that the uncertainties in rate constants for some reactions (e.g., a factor of 10 for R3) are considerably higher than those for other reactions (e.g., 25% for R6 and R7 and a factor of 3.2 for R1), the sensitivity coefficients for each reaction, $\partial \ln(X_i)/\partial \ln(k_j)$, shown in Figure 5a were multiplied by their respective uncertainties, $\sigma_{\ln(k_j)}$, to give uncertainty-weighted sensitivity coefficients (Figure 5b), which reflect the uncertainty in predictions of the mole fraction of a particular species i due to the uncertainty in the rate constant for reaction j. These results indicate the significance of R3 in this system as it is both highly influential and uncertain.

To further explore the influence of R3 on predictions, model predictions were also performed using modified versions of the model of Glarborg et al.[11] that employ a range of values for k_3 within its uncertainty limits (×1/2 and ×1/10) or that employ a value of $k_3 = 0$ (Figure 6). The results in Figure 6 confirm that variation of k_3 within its uncertainty limits yields significant variation in the predicted NO mole fraction. In fact, model predictions of NO become consistent with experimental measurements if k_3 is reduced by a factor of ∼10 from the estimate from Dean and Bozzelli.[29] Reduced values of k_3 would also yield modest improvements in the agreement between model predictions and experimental measurements for N_2O and NH_3. Interestingly, flux and sensitivity analysis performed without R3 in Figures 4 and 5 suggest different controlling pathways—without R3, NH_2 is primarily consumed by reactions with O (R8), H (R9), and NH (R10) instead of N_2O (R3), and NO is primarily produced by reactions involving HNO such as

$$\mathrm{HNO(+M)} \Leftrightarrow \mathrm{NO + H(+M)} \qquad (11)$$

instead of NH_2 (i.e., R3).

To ascertain the extent to which the previous validation data sets have provided tests of R3, which appears to be a key element of submodels for NH_3/N_2O kinetics, simulations with

https://doi.org/10.1021/acs.energyfuels.1c01544
Energy Fuels 2021, 35, 13338−13348

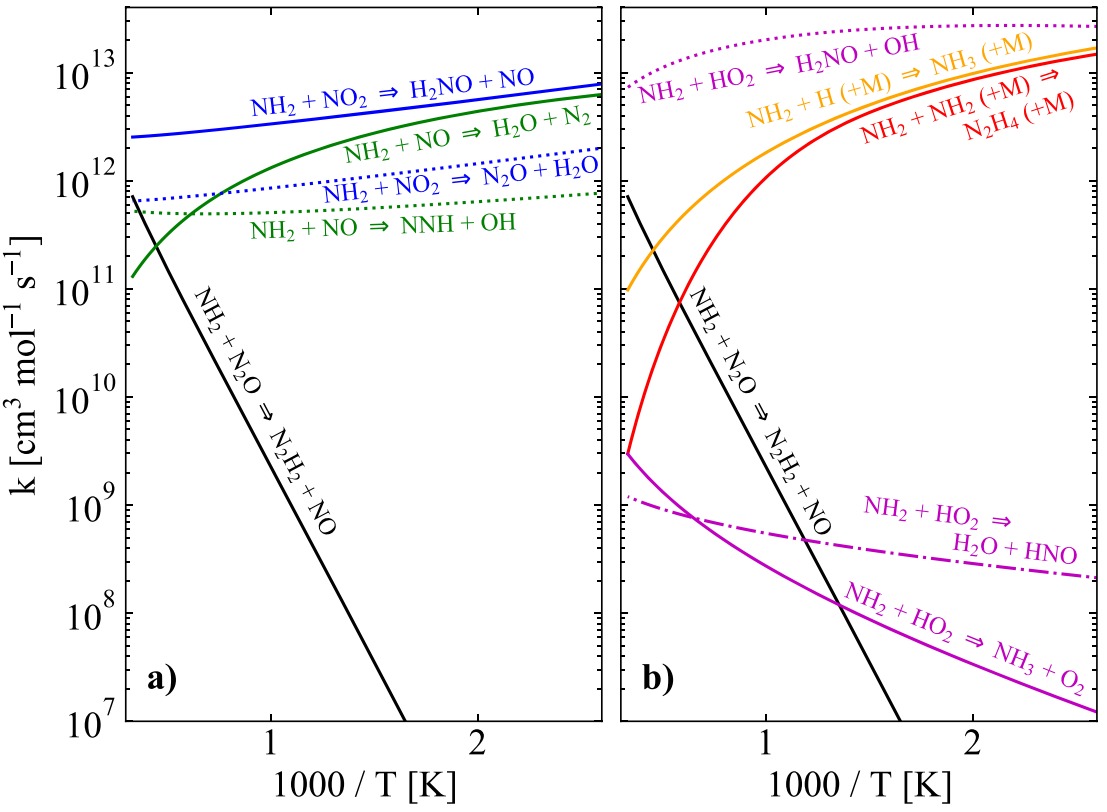

Figure 8. Comparison of rate constants between R3 (solid black line) and competing NH_2 reaction channels known to be important during (a) the SNCR of nitrogen oxides (NO/NO_2) and (b) the ignition of NH_3 at lower/intermediate temperatures. Values are taken from Glarborg et al.[11]

and without R3 were performed for a comprehensive set of NH_3/NO_x kinetic data.[12,32,37,65] This data set consists of flow reactor, JSR, and shock tube ignition delay measurements that span a temperature range of 900−2000 K and a pressure range of 1−30 atm. Model predictions with and without R3, shown in Figure 7, are nearly identical—indicating that previous validation data sets have not tested this particular reaction.

To identify combustion systems that are likely affected by R3, its rate constant was compared against the rate constants of competing reactions of NH_2 that are known to be important during the Selective Non-Catalytic Reduction (SNCR) of nitrogen oxides and the ignition of NH_3 at low and intermediate temperatures using the values of Glarborg et al.[11] (shown in Figure 8).

As indicated in Figure 8a, rate constants of $NH_2 + NO/NO_2$ reactions are orders of magnitude larger than the rate constant of R3 ($NH_2 + N_2O$), which would suggest that R3 is likely only important when the N_2O mole fraction is ∼1000 times higher than the NO and NO_2 mole fractions at 1000 K (and ∼10−100 times higher at 2000 K). Similar trends are shown in Figure 8b for the NH_2 + $NH_2/HO_2/H$ reactions. Many applications involving NH_3, such as its use in the thermal $DeNO_x$ process and its potential use as an alternative fuel, often involve large mole fractions of radicals ($NO/NO_2/NH_2/HO_2/H$), whose reactions with NH_2 compete with R3 and are therefore unlikely to be sensitive to R3. That said, certain combustion environments either quickly form or initially contain large mole fractions of N_2O and therefore may be influenced by this reaction—including, for example, the thermal initiation of nitrogen-rich energetic materials, the formation and reduction of N_2O in fluidized bed combustion, and reduction of N_2O by NH_3. While the role of R3 in these combustion systems has yet to be firmly established, the present results indicate that more accurate quantification of k_3 would improve current submodels for NH_3/N_2O kinetics and contribute to the development of comprehensive models for NH_3 kinetics that can be reliably applied to the full range of highly varied applications involving NH_3.

Equivalent analyses with other models (shown in full in the Supporting Information), which also show the importance of R3 at the present conditions, are qualitatively similar—with the notable exception being the additional importance of R11 in predicted NO formation. The other models, which all use higher values of k_8 than in Glarborg et al.,[11] predict a much larger fraction of NO production from the decomposition of HNO (R11), which is primarily formed via R8, and therefore yield NO/N_2O ratios that differ from the $k_3/(k_6 + k_7)$ quasi-steady-state estimate based solely on formation by R3 and consumption by R6−R7. Reduced values of k_3 still improve the agreement between predicted and measured NO but are insufficient to resolve differences between predictions and measurements for many of the models. Interestingly, for models with reduced values of k_3, the remaining disagreement between predictions and measurements is roughly correlated with the values of k_8 used in each model, which differ by a factor of 4. Like R3, R8 has not received much recent attention, with models apparently relying on a personal communication cited in ref 30 or theoretical estimates based on QRRK calculations[66] that are not expected to be quantitatively accurate. However, unlike R3, R8 also plays a role in predictions of previous validation data (e.g., flames[23]). Based on the variability in rate constants among various

https://doi.org/10.1021/acs.energyfuels.1c01544
Energy Fuels 2021, 35, 13338−13348

models and lack of reliable values, future investigation of R8 would be also appear to be worthwhile.

CONCLUDING REMARKS

Experimental measurements of N_2O, NO, and NH_3 were performed for an $NH_3/N_2O/N_2$ mixture over a range of intermediate temperatures to address gaps in previous validation data sets for nitrogen kinetics. Comparisons of recent kinetic models against the present measurements reveal significant differences, particularly for NO. Flux analysis, uncertainty-weighted sensitivity analysis, and other modeling analyses identified the role of the $N_2O + NH_2 = N_2H_2 + NO$ (R3) reaction, on which recent kinetic models[11,23,24,45,46] all rely on the same rate constant estimate[29] that appears to have remained untested in previous validation data sets for NH_3 kinetics. Given that reduced values of k_3 (within its uncertainty) alone were sufficient to achieve consistency among experimental measurements and model predictions for NO for some kinetic models, improved quantification of k_3 in future studies appears to be worthwhile. In this regard, preliminary theoretical calculations (Stephen Klippenstein, personal communication), which find the reaction barrier of R3 to be 22 kcal/mol (roughly 5 kcal/mol higher than the activation energy of the aforementioned estimate[29] for R3 using the thermochemistry from Glarborg et al.[11]), support the notion that k_3 is likely overestimated in present kinetic models.

That said, even if k_3 were significantly lower than earlier estimates, differences between model predictions and experimental data would still remain for N_2O and NH_3 (and for NO for some kinetic models). As indicated in Figure 5, the other influential reactions in model predictions at the present conditions are often among the most important reactions to predictions of other nitrogen kinetics systems, and their kinetic sensitivity coefficients (and rankings) depend on the values of the rate constants themselves—such that unraveling remaining discrepancies may require simultaneous consideration of the other nitrogen kinetics validation data as well as nonlinearities in the sensitivity coefficients to kinetic parameters. In that regard, we anticipate that our future planned studies applying our MultiScale Informatics approach[47,67,68] to previous experimental and theoretical data for nitrogen kinetics may be useful in unraveling the remaining discrepancies.

ASSOCIATED CONTENT

Supporting Information

The Supporting Information is available free of charge at https://pubs.acs.org/doi/10.1021/acs.energyfuels.1c01544.

Tabulated experimental data; modeling analyses using other kinetic models (PDF)

AUTHOR INFORMATION

Corresponding Author

Michael P. Burke − *Department of Mechanical Engineering and Department of Chemical Engineering and Data Science Institute, Columbia University, New York, New York 10027, United States;* orcid.org/0000-0002-1939-7824; Email: mpburke@columbia.edu

Authors

Rodger E. Cornell − *Department of Mechanical Engineering, Columbia University, New York, New York 10027, United States; U.S. Army DEVCOM AC, Detonation Physics and Experimental Research Branch, Picatinny Arsenal, Wharton, New Jersey 07806, United States*

Mark C. Barbet − *Department of Mechanical Engineering, Columbia University, New York, New York 10027, United States*

Complete contact information is available at: https://pubs.acs.org/10.1021/acs.energyfuels.1c01544

Notes

The authors declare no competing financial interest.

ACKNOWLEDGMENTS

The authors thank the Department of Defense Science, Mathematics, and Research for Transformation (SMART) program, the FY20 U.S. Army DEVCOM AC Independent Laboratory In-house Research (ILIR) program, the FY21 U.S. Army DEVCOM AC Environmental Quality Basic Research (EQBR) program, and the National Science Foundation Combustion and Fire Systems program (CBET-1944004) for funding and continued support. The authors would also like to thank Stephen Klippenstein for sharing the results from his preliminary calculations of R3.

REFERENCES

(1) Valera-Medina, A.; Xiao, H.; Owen-Jones, M.; David, W. I.; Bowen, P. Ammonia for power. *Prog. Energy Combust. Sci.* **2018**, *69*, 63−102.

(2) Valera-Medina, A.; Amer-Hatem, F.; Azad, A.; Dedoussi, I.; De Joannon, M.; Fernandes, R.; Glarborg, P.; Hashemi, H.; He, X.; Mashruk, S.; et al. Review on ammonia as a potential fuel: from synthesis to economics. *Energy Fuels* **2021**, *35*, 6964−7029.

(3) Erisman, J. W.; Sutton, M. A.; Galloway, J.; Klimont, Z.; Winiwarter, W. How a century of ammonia synthesis changed the world. *Nat. Geosci.* **2008**, *1*, 636−639.

(4) Bernet, N.; Béline, F. Challenges and innovations on biological treatment of livestock effluents. *Bioresour. Technol.* **2009**, *100*, 5431−5436.

(5) Randall, D. J.; Tsui, T. Ammonia toxicity in fish. *Mar. Pollut. Bull.* **2002**, *45*, 17−23.

(6) Felipo, V.; Butterworth, R. F. Neurobiology of ammonia. *Prog. Neurobiol.* **2002**, *67*, 259−279.

(7) Kobayashi, H.; Hayakawa, A.; Somarathne, K. K. A.; Okafor, E. C. Science and technology of ammonia combustion. *Proc. Combust. Inst.* **2019**, *37*, 109−133.

(8) Ho, P. T.; Townes, C. H. Interstellar ammonia. *Annu. Rev. Astron. Astrophys.* **1983**, *21*, 239−270.

(9) Lu, Z.-m.; Lu, J.-d Influences of O_2 concentration on NO reduction and N_2O formation in thermal deNOx process. *Combust. Flame* **2009**, *156*, 1303−1315.

(10) Glarborg, P.; Dam-Johansen, K.; Miller, J. A.; Kee, R. J.; Coltrin, M. E. Modeling the thermal DENOx process in flow reactors. Surface effects and nitrous oxide formation. *Int. J. Chem. Kinet.* **1994**, *26*, 421−436.

(11) Glarborg, P.; Miller, J. A.; Ruscic, B.; Klippenstein, S. J. Modeling nitrogen chemistry in combustion. *Prog. Energy Combust. Sci.* **2018**, *67*, 31−68.

(12) Kasuya, F.; Glarborg, P.; Johnsson, J. E.; Dam-Johansen, K. The thermal $DeNO_x$ process: Influence of partial pressures and temperature. *Chem. Eng. Sci.* **1995**, *50*, 1455−1466.

(13) Honorien, J.; Fournet, R.; Glaude, P.-A.; Sirjean, B. Theoretical study of the gas-phase thermal decomposition of urea. *Proc. Combust. Inst.* **2021**, *38*, 355−364.

(14) Cornell, R. E.; Barbet, M. C.; Burke, M. P. Automated discovery of influential chemically termolecular reactions in energetic material combustion: A case study for RDX. *Proc. Combust. Inst.* **2021**, *38*, 787−794.

(15) Cornell, R. E.; Barbet, M. C.; Burke, M. P. Experimentally Testing the Performance of Small Molecule Chemistry Relevant to Energetic Materials. *2020 Spring Technical Meeting of the Eastern States Section of the Combustion Institute*; 2020; p 2A07.
(16) Boldyrev, V. Thermal decomposition of ammonium perchlorate. *Thermochim. Acta* **2006**, *443*, 1−36.
(17) Oxley, J. C.; Smith, J. L.; Rogers, E.; Yu, M. Ammonium nitrate: thermal stability and explosivity modifiers. *Thermochim. Acta* **2002**, *384*, 23−45.
(18) Samuels, P.; Spangler, K.; Iwaniuk, D.; Cornell, R.; Baker, E. L.; Stiel, L. I. Detonation performance analyses for recent energetic molecules. *AIP Conference Proceedings*; 2018; p 150033.
(19) Hupa, M.; Karlström, O.; Vainio, E. Biomass combustion technology development-It is all about chemical details. *Proc. Combust. Inst.* **2017**, *36*, 113−134.
(20) Montes, F.; Meinen, R.; Dell, C.; Rotz, A.; Hristov, A. N.; Oh, J.; Waghorn, G.; Gerber, P. J.; Henderson, B.; Makkar, H.; et al. SPECIAL TOPICS-mitigation of methane and nitrous oxide emissions from animal operations: II. A review of manure management mitigation options. *J. Anim. Sci.* **2013**, *91*, 5070−5094.
(21) Winter, F.; Wartha, C.; Hofbauer, H. NO and N_2O formation during the combustion of wood, straw, malt waste and peat. *Bioresour. Technol.* **1999**, *70*, 39−49.
(22) Glarborg, P.; Hashemi, H.; Cheskis, S.; Jasper, A. W. On the Rate Constant for $NH_2 + HO_2$ and Third-Body Collision Efficiencies for $NH_2 + H$ (+ M) and $NH_2 + NH_2$ (+ M). *J. Phys. Chem. A* **2021**, *125*, 1505−1516.
(23) Stagni, A.; Cavallotti, C.; Arunthanayothin, S.; Song, Y.; Herbinet, O.; Battin-Leclerc, F.; Faravelli, T. An experimental, theoretical and kinetic-modeling study of the gas-phase oxidation of ammonia. *Reaction Chemistry & Engineering* **2020**, *5*, 696−711.
(24) Han, X.; Lubrano Lavadera, M.; Konnov, A. A. An experimental and kinetic modeling study on the laminar burning velocity of $NH_3 + N_2O$ + air flames. *Combust. Flame* **2021**, *228*, 13−28.
(25) Miller, J. A.; Bowman, C. T. Mechanism and modeling of nitrogen chemistry in combustion. *Prog. Energy Combust. Sci.* **1989**, *15*, 287−338.
(26) Haynes, B. The oxidation of hydrogen cyanide in fuel-rich flames. *Combust. Flame* **1977**, *28*, 113−121.
(27) Klippenstein, S. J.; Harding, L. B.; Glarborg, P.; Miller, J. A. The role of NNH in NO formation and control. *Combust. Flame* **2011**, *158*, 774−789.
(28) Skreiberg, Ø.; Kilpinen, P.; Glarborg, P. Ammonia chemistry below 1400 K under fuel-rich conditions in a flow reactor. *Combust. Flame* **2004**, *136*, 501−518.
(29) Dean, A. M.; Bozzelli, J. W. *Gas-Phase Combustion Chemistry*; Springer: New York, 2000; pp 125−341.
(30) Miller, J. A.; Smooke, M. D.; Green, R. M.; Kee, R. J. Kinetic modeling of the oxidation of ammonia in flames. *Combust. Sci. Technol.* **1983**, *34*, 149−176.
(31) Lindstedt, R.; Lockwood, F.; Selim, M. A detailed kinetic study of ammonia oxidation. *Combust. Sci. Technol.* **1995**, *108*, 231−254.
(32) Mathieu, O.; Petersen, E. L. Experimental and modeling study on the high-temperature oxidation of Ammonia and related NO_x chemistry. *Combust. Flame* **2015**, *162*, 554−570.
(33) Bian, J.; Vandooren, J.; Van Tiggelen, P. Experimental study of the structure of an ammonia-oxygen flame. *Symp. (Int.) Combust., [Proc.]* **1988**, *21*, 953−963.
(34) Mendiara, T.; Glarborg, P. Ammonia chemistry in oxy-fuel combustion of methane. *Combust. Flame* **2009**, *156*, 1937−1949.
(35) Arunthanayothin, S.; Stagni, A.; Song, Y.; Herbinet, O.; Faravelli, T.; Battin-Leclerc, F. Ammonia-methane interaction in jet-stirred and flow reactors: An experimental and kinetic modeling study. *Proc. Combust. Inst.* **2021**, *38*, 345−353.
(36) Alzueta, M. U.; Røjel, H.; Kristensen, P. G.; Glarborg, P.; Dam-Johansen, K. Laboratory study of the $CO/NH_3/NO/O_2$ system: Implications for hybrid reburn/SNCR strategies. *Energy Fuels* **1997**, *11*, 716−723.
(37) Rota, R.; Antos, D.; Zanoelo, E.; Carra, S. Experimental study and kinetic modelling of nitric oxide reduction with ammonia. *Combust. Sci. Technol.* **2001**, *163*, 25−47.
(38) Duo, W.; Dam-Johansen, K.; Østergaard, K. Kinetics of the gas-phase reaction between nitric oxide, ammonia and oxygen. *Can. J. Chem. Eng.* **1992**, *70*, 1014−1020.
(39) Vandooren, J.; Bian, J.; Van Tiggelen, P. Comparison of experimental and calculated structures of an ammonia nitric oxide flame. Importance of the NH_2 + NO reaction. *Combust. Flame* **1994**, *98*, 402−410.
(40) Mei, B.; Ma, S.; Zhang, X.; Li, Y. Characterizing ammonia and nitric oxide interaction with outwardly propagating spherical flame method. *Proc. Combust. Inst.* **2021**, *38*, 2477−2485.
(41) Drummond, L.; Hiscock, S. Shock-initiated exothermic reactions. II. The oxidation of ammonia. *Aust. J. Chem.* **1967**, *20*, 825−836.
(42) Salimian, S.; Hanson, R.; Kruger, C. Ammonia oxidation in shock-heated NH_3-N_2O-Ar mixtures. *Combust. Flame* **1984**, *56*, 83−95.
(43) Venizelos, D.; Sausa, R. Detailed chemical kinetics studies of an NH_3/N_2O/Ar flame by laser-induced fluorescence, mass spectrometry, and modeling. *Proc. Combust. Inst.* **2000**, *28*, 2411−2418.
(44) Kilpinen, P.; Hupa, M. Homogeneous N_2O chemistry at fluidized bed combustion conditions: A kinetic modeling study. *Combust. Flame* **1991**, *85*, 94−104.
(45) Zhang, Y.; Mathieu, O.; Petersen, E. L.; Bourque, G.; Curran, H. J. Assessing the predictions of a NO_x kinetic mechanism on recent hydrogen and syngas experimental data. *Combust. Flame* **2017**, *182*, 122−141.
(46) Shrestha, K. P.; Seidel, L.; Zeuch, T.; Mauss, F. Detailed kinetic mechanism for the oxidation of ammonia including the formation and reduction of nitrogen oxides. *Energy Fuels* **2018**, *32*, 10202−10217.
(47) Burke, M. P. Harnessing the combined power of theoretical and experimental data through multiscale informatics. *Int. J. Chem. Kinet.* **2016**, *48*, 212−235.
(48) Herbinet, O.; Marquaire, P.-M.; Battin-Leclerc, F.; Fournet, R. Thermal decomposition of n-dodecane: Experiments and kinetic modeling. *J. Anal. Appl. Pyrolysis* **2007**, *78*, 419−429.
(49) Herbinet, O.; Battin-Leclerc, F. Progress in understanding low-temperature organic compound oxidation using a jet-stirred reactor. *Int. J. Chem. Kinet.* **2014**, *46*, 619−639.
(50) Matras, D.; Villermaux, J. Un réacteur continu parfaitement agité par jets gazeux pour l'étude cinétique de réactions chimiques rapides. *Chem. Eng. Sci.* **1973**, *28*, 129−137.
(51) Ayass, W. W. Mixing in Jet-Stirred Reactors with Different Geometries. Ph.D. Thesis, King Abdullah University of Science and Technology Thuwal, Kingdom of Saudi Arabia, 2013.
(52) Ayass, W. W.; Nasir, E. F.; Farooq, A.; Sarathy, S. M. Mixing-structure relationship in jet-stirred reactors. *Chem. Eng. Res. Des.* **2016**, *111*, 461−464.
(53) David, R.; Matras, D. Règies de construction et d'extrapolation des réacteurs auto-agités par jets gazeux. *Can. J. Chem. Eng.* **1975**, *53*, 297−300.
(54) Marquaire, P.-M.; Wörner, R.; Rambaud, P.; Baronnet, F. High temperature oxidation of dioxins. *Organohalogen Compd.* **1999**, *40*, 519−522.
(55) Herbinet, O.; Sirjean, B.; Bounaceur, R.; Fournet, R.; Battin-Leclerc, F.; Scacchi, G.; Marquaire, P.-M. Primary mechanism of the thermal decomposition of tricyclodecane. *J. Phys. Chem. A* **2006**, *110*, 11298−11314.
(56) Marrodán, L.; Song, Y.; Lubrano Lavadera, M.; Herbinet, O.; De Joannon, M.; Ju, Y.; Alzueta, M. U.; Battin-Leclerc, F. Effects of Bath Gas and NO_x Addition on n-Pentane Low-Temperature Oxidation in a Jet-Stirred Reactor. *Energy Fuels* **2019**, *33*, 5655−5663.
(57) Azay, P.; Côme, G.-M. Temperature gradients in a continuous flow stirred tank reactor. *Ind. Eng. Chem. Process Des. Dev.* **1979**, *18*, 754−756.
(58) Dagaut, P.; Cathonnet, M.; Rouan, J.; Foulatier, R.; Quilgars, A.; Boettner, J.; Gaillard, F.; James, H. A jet-stirred reactor for kinetic

studies of homogeneous gas-phase reactions at pressures up to ten atmospheres (1 MPa). *J. Phys. E: Sci. Instrum.* **1986**, *19*, 207.
(59) Goodwin, D. G.; Moffat, H. K.; Speth, R. L. *Cantera: An Object-Oriented Software Toolkit for Chemical Kinetics, Thermodynamics, and Transport Processes*, Version 2.4.0; 2018.
(60) Smith, G.; Tao, Y.; Wang, H. *Foundational Fuel Chemistry Model*, Version 1.0; 2016; http://nanoenergy.stanford.edu/ffcm1.
(61) Tsang, W.; Hampson, R. Chemical kinetic data base for combustion chemistry. Part I. Methane and related compounds. *J. Phys. Chem. Ref. Data* **1986**, *15*, 1087−1279.
(62) Tsang, W.; Herron, J. T. Chemical kinetic data base for propellant combustion I. Reactions involving NO, NO_2, HNO, HNO_2, HCN and N_2O. *J. Phys. Chem. Ref. Data* **1991**, *20*, 609−663.
(63) Baulch, D.; Bowman, C. T.; Cobos, C. J.; Cox, R.; Just, T.; Kerr, J.; Pilling, M.; Stocker, D.; Troe, J.; Tsang, W.; et al. Evaluated kinetic data for combustion modeling: supplement II. *J. Phys. Chem. Ref. Data* **2005**, *34*, 757−1397.
(64) Cohen, N.; Westberg, K. Chemical kinetic data sheets for high-temperature reactions. Part II. *J. Phys. Chem. Ref. Data* **1991**, *20*, 1211−1311.
(65) Arai, N.; Higashi, T.; Hasatani, M.; Sugiyama, S. Formation of thermal NO_x in a binary system of nitrogen and oxygen. *Int. Chem. Eng.* **1978**, *18*, 661−665.
(66) Sumathi, R.; Sengupta, D.; Nguyen, M. T. Theoretical study of the H_2 + NO and related reactions of $[H_2NO]$ isomers. *J. Phys. Chem. A* **1998**, *102*, 3175−3183.
(67) Burke, M. P.; Klippenstein, S. J.; Harding, L. B. A quantitative explanation for the apparent anomalous temperature dependence of OH + HO_2 = H_2O + O_2 through multi-scale modeling. *Proc. Combust. Inst.* **2013**, *34*, 547−555.
(68) LaGrotta, C. E.; Barbet, M. C.; Lei, L.; Burke, M. P. Towards a high-accuracy kinetic database informed by theoretical and experimental data: CH_3 + HO_2 as a case study. *Proc. Combust. Inst.* **2021**, *38*, 1043−1051.

https://doi.org/10.1021/acs.energyfuels.1c01544
Energy Fuels 2021, 35, 13338−13348